Regime Mapping and Parameter Importance in Stochastic ABM of Behavioral Sink*

Federico Carucci[1,2], Leonardo Mascagni[1,2], Lorenzo Gastaldo[1,2], Luca Moroni[1,2] and Francesco Bertolotti[2,3,*]

[1]School of Industrial Engineering, Cattaneo University – LIUC, Italy
[2]Intelligence, Complexity, and Technology Lab (ICT Lab), University Cattaneo – LIUC, Italy
[3]Università Cattolica di Milano, Department of Philosophy, L. Gemelli 1 - 20123 Milano, Italy

Abstract

Population collapse is most commonly attributed to resource scarcity, predation, and disease, yet a distinct class of endogenous mechanisms produces demographic decline independently of these conventional drivers. Overcrowding represents one such mechanism, in which perceived density generates accumulated stress, stress suppresses reproduction, and reduced reproduction produces demographic decline even in the absence of resource scarcity — a dynamic first described by Calhoun as the behavioral sink. Despite being empirically documented across taxa, the geometry of the parameter space in which this transition occurs remains formally uncharacterised. We use a stochastic individual-based agent-based model to conduct a large-scale parametric exploration of 50,000 simulations and map the boundary between survival and collapse regimes across an eight-dimensional parameter space. Two response variables are analysed: extinction probability and collapse severity. A random forest metamodel is used to assess parameter importance through permutation-based ranking on a held-out test set. Mortality and baseline fertility emerge as the dominant predictors of collapse outcomes, while stress accumulation, total space, and fertility suppression contribute marginally, and initial population size, number of nodes, and stress decay are indistinguishable from zero within the explored domain. The transition from persistence to extinction is not abrupt but preceded by a broad region of severe demographic decline. The parameter space partitions into three qualitatively distinct regimes — direct collapse, gradual decline, and overshoot collapse — in which the same causal mechanism produces profoundly different demographic histories depending on the location in the baseline fertility–mortality plane. These findings support the interpretation of the behavioral sink as a general endogenous collapse mechanism and provide the first systematic characterisation of the geometry of its critical boundary in parameter space.

Keywords

Agent-based model, Behavioral sink, Population collapse, Tipping points, Overcrowding

1. Introduction

Population collapse is most commonly attributed to resource scarcity, predation, and disease, yet a distinct class of endogenous collapse exists in which demographic decline occurs independently of these conventional drivers [1, 2]. Overcrowding represents one such mechanism, first documented by Calhoun in controlled rodent experiments in which confined populations collapsed despite abundant material resources, as increasing density produced social disintegration and reproductive failure [3, 4]. Analogous patterns have been documented in wild meadow voles, where elevated social density suppresses GnRH expression through epigenetic modifications [5], and in gregarious cave-dwelling bats, where overcrowding increases aggression and reduces reproductive success [6]. These dynamics are of growing relevance in a global context in which spatial compression represents a documented and increasing trend for both animal and human populations [7, 8].

WOA2026, the 27th Workshop From Objects to Agents, June 15–17, 2026, Salerno, Italy
*You can use this document as the template for preparing your publication. We recommend using the latest version of the ceurart style.
*Corresponding author.
†These authors contributed equally.
fcarucci@liuc.it (F. Carucci); fbertolotti@liuc.it (F. Bertolotti)
0000-0003-1274-9628 (F. Bertolotti)


The mechanism underlying these phenomena unfolds as a causal chain in which perceived density generates accumulated stress, stress suppresses reproduction, and reduced reproduction produces demographic decline even in the absence of resource scarcity [9, 10, 11]. This chain is intrinsically history-dependent, as stress accumulates through allostatic load mechanisms in which individual responses depend on the entire preceding trajectory of exposure [10]. The distinction between physical density and perceived crowding is in this sense fundamental, since identical densities can produce profoundly different behavioural and physiological responses depending on the social context in which individuals operate [12, 13]. Despite being empirically documented across taxa, the demographic conditions under which the behavioral sink emerges as a system-level collapse — and the geometry of the parameter space in which this transition occurs — remain formally uncharacterised.

A recent meta-model proposed a minimal representation of this mechanism, implemented both as an equation-based model and as an agent-based model, and calibrated on the Universe 25 experiment [14]. The model reproduces the empirical growth-collapse trajectory with low error and shows that the ABM generates a structured ensemble of trajectories organised into a limited number of recurrent regimes, whose dominant regime is consistent with the empirical data and stable under local parameter perturbations [14]. This analysis is however conducted at a single point in the parameter space, corresponding to the configuration calibrated on the Calhoun experiment, and provides no information on how the dynamic structure of the model organises itself as the baseline demographic conditions vary.

In stochastic ABMs, understanding model behaviour requires a systematic exploration of the parameter space such that the organisation of dynamic regimes can be identified as a function of the inputs, since simulations conducted at a single point are insufficient to characterise the global structure of the system [15, 16]. This need is particularly relevant for models in which individual stochasticity generates multimodal trajectory distributions, as the dominant regime and its relative frequency can reorganise nonlinearly across the parameter space in ways that local sensitivity analysis cannot detect [17, 16]. Establishing the phase diagram of an ABM — that is, identifying the regions of parameter space in which the system exhibits qualitatively distinct regimes and locating the boundaries between them — constitutes a necessary prerequisite for any predictive or comparative use of the model [17]. This prerequisite is unmet for the behavioral sink ABM of Carucci and Bertolotti, whose parameter space remains unexplored beyond the single calibrated configuration.

The present work maps the boundary between survival and collapse regimes in the parameter space of the behavioral sink ABM and identifies the parameters that govern its position. The exploration is conducted over 50,000 simulations generated through stochastic sampling of a discretised eight-dimensional parameter space. The results show that baseline fertility and mortality are the dominant predictors of collapse outcomes, while the remaining parameters exert marginal influence within the explored domain. The transition from persistence to extinction is preceded by an extended region of severe demographic decline, and the parameter space partitions into three qualitatively distinct regimes — direct collapse, gradual decline, and overshoot collapse — in which the same causal mechanism produces profoundly different demographic histories depending on the location in the (n, m) plane. These findings provide the first systematic characterisation of the geometry of the critical boundary in the parameter space of a formal model of the behavioral sink.

2. Background

The behavioral sink was first documented by Calhoun in a series of confined rodent experiments, of which Universe 25 is the most cited [3, 4]. As density rose in a closed environment with unlimited resources, the colony underwent progressive social disintegration, in which the breakdown of parental care, abnormal aggression, and social withdrawal reduced reproductive success to the point of complete demographic collapse. Similar patterns have been documented across distinct taxa. Gregarious cave-dwelling bats show increased aggression and reduced reproductive activity under high-density conditions [6]. Wild meadow voles show density-dependent downregulation of the reproductive axis,

including reduced GnRH expression and increased DNA methylation under elevated social density [5]. In Arctic lemmings, comparable epigenetic involvement remains a plausible but still unconfirmed hypothesis [18]. Rhesus macaques develop measurable physiological stress responses and reorganised social structures under long-term crowding [19, 20], while small rodents show density-induced neuroendocrine alterations that directly suppress reproductive function [21]. More broadly, comparative work across mammalian social systems suggests that fertility costs associated with group living and elevated social density represent a general phenomenon rather than a taxon-specific response [22].

Understanding these patterns requires distinguishing density, an objective and quantifiable measure of the number of individuals per unit of space, from crowding, which represents its subjective and contextual translation, in which the same physical density can generate profoundly different behavioural and physiological responses depending on the social and cultural context in which individuals operate [12, 23, 13]. This distinction implies that it is not density itself that produces dysfunction, but density perceived as excessive relative to the expectations and coping capacities of the system. The biological mechanisms through which this perception operates—including stress sensitization [24], gestational transmission of allostatic load [25], and neuroendocrine suppression of the reproductive axis [5]—provide the motivational background for the modelling framework developed here, even though they are not represented at the level of individual mechanisms in the model.

The stress generated by crowding does not operate as an instantaneous response but accumulates over time through allostatic load mechanisms, producing a persistent internal condition whose severity increases with the duration of exposure [10, 11]. This property renders the system intrinsically history-dependent, in which the current response of an individual depends not only on present density but on the entire preceding trajectory of exposure. In ecological systems, stress accumulation has been documented in contexts of prolonged social crowding, where suppression of the reproductive axis occurs through density-induced modifications of GnRH expression [5], and more broadly through behavioural and physiological alterations associated with chronic stress [9].

The causal chain that emerges, linking perceived crowding to stress accumulation and reproductive suppression, constitutes a nonlinear and history-dependent feedback such that the system becomes susceptible to critical transitions, in which small parametric variations produce qualitatively irreversible changes in demographic dynamics. Systems with this structure can exhibit multiple alternative stable regimes, in which a gradual change in a control parameter is sufficient to push the system past a threshold beyond which recovery becomes unlikely, a transition known as a tipping point [26, 27]. In ecological and socio-ecological systems, such transitions have been documented across contexts as diverse as the collapse of lake ecosystems, the desertification of semi-arid zones, and the decline of keystone populations [28, 29]. Their preventive identification remains an open problem, since precursor signals are typically weak and the system appears stable until shortly before the transition [30].

Mapping the parameter space of a formal model represents a standard approach to characterising the geometry of such transitions in complex systems [17]. In stochastic agent-based models, this requires exploring how the distribution of possible system trajectories reorganises as input parameters vary, since the location and sharpness of the critical boundary cannot be inferred from simulations conducted at a single point [16].

3. Materials and Methods

3.1. Model

The ABM is a discrete-time stochastic individual-based model defined on z spatial nodes. The total available space R is uniformly partitioned across nodes, so that the reference local capacity is $r = R/z$. At $t = 0$, P_0 individuals are assigned independently and uniformly to the z nodes, and each individual is initialised with stress s_0. Each individual i is described by two state variables, its node $x_i \in \{1, \dots, z\}$ and its stress level $s_i(t) \geq 0$. No migration is implemented, so that the node of an individual remains fixed throughout its lifetime and offspring inherit the parent's node. Spatial heterogeneity therefore emerges only from the initial allocation and from the subsequent local demographic dynamics.

At each time step, the model computes node occupancy

$$N_j(t) = \sum_i \mathbf{1}(x_i = j), \tag{1}$$

total population

$$P_t = \sum_{j=1}^{z} N_j(t), \tag{2}$$

and mean population stress

$$S_t = \frac{1}{P_t} \sum_i s_i(t), \tag{3}$$

with $S_t = 0$ if $P_t = 0$. For each node the model also records the local mean stress.

Individuals are then updated sequentially. For individual i in node $j = x_i$, stress accumulation is governed by

$$A_i(t) = c\left(\frac{N_j(t)}{r}\right)(1 + s_i(t)), \tag{4}$$

where c controls the intensity of crowding-induced stress. Since the subjective perception of crowding cannot be parameterised directly at the individual level, local density relative to capacity, $N_j(t)/r$, serves here as an operational proxy for experienced crowding, in line with the minimal modelling strategy of Carucci and Bertolotti [14]. Stress is then updated as

$$s_i^*(t) = \max\{0,\ (s_i(t) + A_i(t))(1 - d)\}, \tag{5}$$

where $d \in [0, 1]$ is the stress decay parameter. This formulation renders stress both density-dependent and history-dependent, since previously accumulated stress amplifies further accumulation.

Reproduction is stochastic and stress-dependent. After the stress update, individual i reproduces with probability

$$p_i^{\text{birth}}(t) = \frac{n}{1 + k\, s_i^*(t)}, \tag{6}$$

where n is the baseline fertility parameter and k modulates the strength of fertility suppression by stress. When reproduction occurs, one offspring is created in node x_i and assigned stress value $s_i^*(t)$, capturing a minimal form of intergenerational stress transmission. Mortality is independent and occurs with probability m for each individual at each step; individuals selected for death are removed at the end of the time step. The implementation uses a sequential within-step update, so newborn individuals are appended immediately and may themselves be processed later in the same step.

The model parameters are therefore T (time horizon), c (stress accumulation), m (mortality probability), n (baseline fertility), d (stress decay), k (fertility suppression by stress), R (total space), P_0 (initial population), s_0 (initial stress), and z (number of nodes). The individual-level state variables are x_i and $s_i(t)$; the aggregate state variables are $N_j(t)$, P_t, and S_t. In this form, the ABM isolates the demographic consequences of local crowding, cumulative stress, and stress-mediated reproductive suppression [14].

3.2. Analysis

The parametric exploration targets the eight model parameters formalised in Table 1. A large-scale exploration was conducted to map the boundary between survival and collapse regimes across the parameter space. Rather than performing an exhaustive grid search, each parameter range was discretised into 20 evenly spaced values and each simulation run was generated by randomly sampling one value per parameter from the corresponding discrete set. This design produces a stochastic coverage of a regular discretised parameter space in which the marginal distribution of each parameter is uniform over its range. In total, 50,000 simulations were conducted, each with time horizon $T = 2500$. A fixed random seed was used to ensure reproducibility. The parameters varied in the exploration and their explored ranges are reported in Table 1.

Table 1
Explored ranges for the eight varied parameters. Each range was discretised into 20 evenly spaced values.

Parameter	Symbol	Min	Max
Baseline fertility	n	1.0×10^{-4}	4.0×10^{-2}
Mortality probability	m	1.0×10^{-4}	1.5×10^{-2}
Initial population	P_0	5	200
Stress accumulation	c	1.0×10^{-4}	8.0×10^{-4}
Stress decay	d	1.0×10^{-8}	6.0×10^{-8}
Fertility suppression	k	10.0	60.0
Total space	R	1000	8000
Number of nodes	z	2	30

Simulation outputs. For each simulation, the full population time series was recorded together with a summary row containing the sampled parameter configuration and a set of derived outcome indicators. When population reached zero, the time series was truncated at the first extinction time, since all subsequent values were necessarily zero. Two output datasets were thereby produced, a time-series dataset containing the population trajectory of each run and a summary dataset containing one row per simulation.

Derived indicators. For each run, peak population was computed as

$$P_{\text{peak}} = \max_t P_t, \tag{7}$$

with corresponding peak time $t_{\text{peak}} = \arg\max_t P_t$. The final population value P_{final} was also recorded. Three response variables were used throughout the analysis. Extinction was encoded as a binary indicator equal to one when $P_{\text{final}} = 0$ within the simulated horizon, capturing whether the population disappears entirely. Collapse severity was defined as

$$\text{collapse\_severity} = 1 - \frac{P_{\text{final}}}{P_{\text{peak}}}, \tag{8}$$

a continuous quantity bounded in $[0, 1]$ that measures the magnitude of post-peak demographic decline regardless of whether extinction occurs. Values close to zero indicate little or no decline from the peak; values close to one indicate severe collapse. The slope at the inflection point was defined as the normalised rate of maximum post-peak decline, computed as

$$\text{slope\_inflection} = \frac{\Delta P_{\min}}{P_{t_{\text{flex}}}}, \tag{9}$$

where $\Delta P_{\min} = \min_t(P_{t+1} - P_t)$ over the post-peak trajectory and $P_{t_{\text{flex}}}$ is the population at the corresponding time step. This indicator captures the sharpness of the collapse independently of its magnitude, and is complementary to collapse severity in characterising the two-stage structure of the transition. The three variables are complementary rather than redundant: extinction identifies whether a population survives at all within the simulated horizon, collapse severity quantifies how strongly it declines from its maximum, and slope at inflection measures how abruptly that decline occurs.

Regime mapping. The simulated outcomes were analysed through empirical maps of the parameter space. For each pair of parameters of interest, a two-dimensional grid was constructed and the mean value of the selected response variable was computed for each cell over all simulations sharing that parameter combination. The resulting heatmaps represent average outcomes conditional on the displayed parameter pair and marginalised over the remaining sampled parameters. Primary maps were constructed in the (n, m) plane; additional maps were produced in the (n, P_0) and (m, P_0) planes to assess whether initial population size displaced the observed transition structure. For extinction

maps, the contour at probability 0.5 was used as an empirical transition boundary between regions of predominantly persistent and predominantly extinct outcomes within the simulated horizon. This boundary is identified operationally within the explored parameter space and does not constitute a formal demonstration of bistability or hysteresis in the dynamical system sense.

Parameter importance. To identify the parameters most strongly associated with collapse severity and extinction, a random forest metamodel was trained using the sampled parameters as predictors and collapse severity as the target variable [16]. The model consisted of 300 estimators trained on 75% of the simulations, with the remaining 25% held out for evaluation. Class imbalance was addressed through balanced class weighting. Importance was estimated by permutation importance on the held-out test set, repeated over 20 permutation rounds, providing a ranking of the relative predictive contribution of each parameter within the explored domain without implying a causal interpretation.

Trajectory visualisation. Full population trajectories were visualised for selected parameter configurations to complement the synthetic regime maps. For three representative values of baseline fertility at fixed mortality, 500 stochastic realisations were generated by sampling the remaining parameters uniformly across their explored ranges. These visualisations show how regions of the parameter space that yield similar summary indicators nonetheless correspond to qualitatively distinct dynamic profiles, and allow the mean peak time $\bar{t}_{\text{peak}}$ to be tracked as fertility varies.

4. Results

The exploration reveals a structured and interpretable organisation of collapse outcomes across the parameter space. Collapse severity is predicted primarily by the core demographic parameters of the model, the transition between persistence and collapse is organised around a well-defined region in the (n, m) plane, and the stochastic trajectories underlying these summary outcomes remain qualitatively coherent with the regime structure identified by the maps. Taken together, these findings indicate that the model does not generate arbitrary variability but a patterned set of outcomes whose geometry can be characterised empirically.

4.1. Parameter importance

The permutation importance analysis identifies mortality m as the dominant predictor of collapse outcomes, with an importance score substantially higher than all remaining parameters (Figure 1). Baseline fertility n ranks second at a considerable distance, while stress accumulation c, total space R, and fertility suppression k contribute marginally and in decreasing order. Initial population P_0, number of nodes z, and stress decay d display importance values indistinguishable from zero within the explored domain. This ranking should be interpreted in predictive rather than causal terms: it does not imply that the remaining parameters are dynamically irrelevant, but that when mortality and fertility vary simultaneously across the sampled configurations, variation in these other parameters contributes less to the out-of-sample prediction of collapse outcomes. The apparent irrelevance of d in particular reflects the finite simulation horizon of $T = 2500$ time steps: d governs the rate at which accumulated stress dissipates over time, and its effect on demographic outcomes is expected to manifest over timescales that exceed the simulated horizon.

4.2. Regime structure in the (n, m) plane

The three panels of Figure 2 provide complementary characterisations of the collapse regime across the (n, m) plane, marginalised over the remaining sampled parameters.

Panel A reports mean collapse severity. The map shows a broad region of severe post-peak demographic decline occupying the high-mortality and low-fertility portion of the plane, with a continuous and nonlinear gradient toward the low-mortality, high-fertility corner. Severe decline is already present

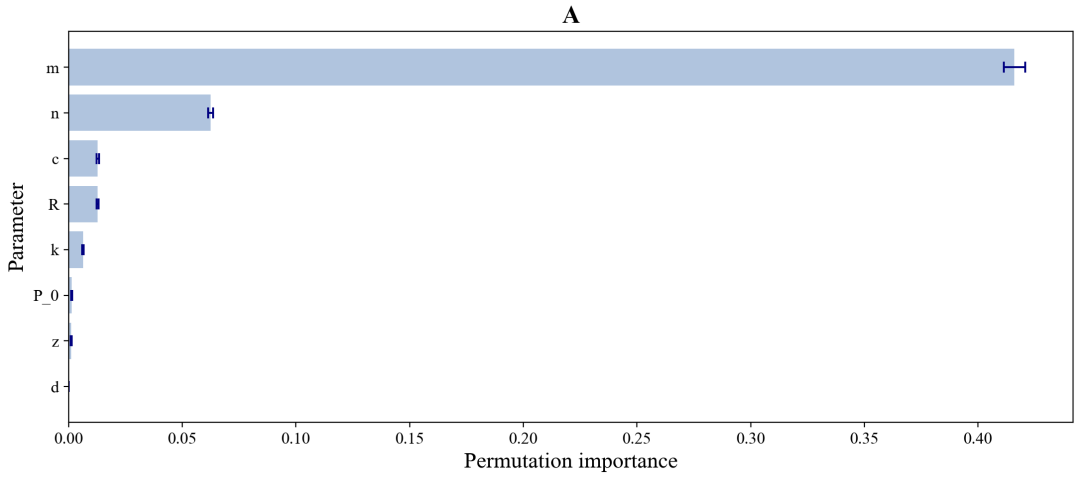

Figure 1: Permutation importance of the eight model parameters with respect to extinction probability, estimated on a held-out test set. Bars represent mean importance across 20 permutation repetitions; error bars denote one standard deviation.

over a wide intermediate region before extinction becomes the dominant outcome, indicating that substantial demographic deterioration can occur even when some individuals persist at the end of the simulated horizon.

Panel B reports the probability of extinction within $T = 2500$ time steps. The transition boundary at $p = 0.50$ identifies a narrow region in the low-n, low-m portion of the plane where small parametric variations produce qualitatively different outcomes: below the boundary persistence is more likely, above it extinction becomes the modal result. The boundary is not linear — higher mortality requires progressively higher baseline fertility for population persistence — a curvature consistent with the stress-mediated reproductive suppression feedback at the core of the behavioral sink mechanism. In regions where extinction is not observed within T, demographic collapse remains probable over longer horizons; the extinction probability reported here is therefore a lower bound conditioned on the simulated horizon rather than a definitive assessment of long-term persistence.

Panel C reports the slope at the inflection point. In the high-n, low-m region the slope approaches zero, indicating that post-peak decline is slow and protracted. Moving toward the high-m, low-n corner the slope becomes increasingly negative, reflecting a collapse that is not only severe but abrupt. Considered jointly, the three panels partition the parameter space into three qualitatively distinct regions: one in which the population does not collapse within the simulated horizon but is likely to do so over longer timescales, one in which it declines gradually, and one in which collapse is both severe and rapid. The transition between persistence and collapse should not be interpreted as a formal proof of bistability or hysteresis in the dynamical-systems sense; it is an empirical boundary identified operationally within the explored parameter space.

4.3. Peak population and role of stress accumulation

Panel A of Figure 3 maps the mean peak population in the (n, m) plane. Peak population increases strongly as baseline fertility rises and mortality declines, producing a markedly nonlinear gradient concentrated in the low-m, high-n corner. This region overlaps with the zone in which $\bar{t}_{\text{peak}}$ approaches or exceeds $T = 2500$, indicating that the population has not yet reached its maximum within the simulated horizon. The high peak population values observed there are therefore not evidence of long-term persistence but reflect trajectories still in their growth phase at termination.

Panels B and C examine the role of the stress accumulation parameter c by mapping extinction probability in the (n, c) and (m, c) planes respectively. In both cases the isolines are nearly vertical with respect to c, indicating that varying c across its entire explored range produces only marginal changes in extinction probability conditional on fixed n or m. The dominant gradient in both panels follows

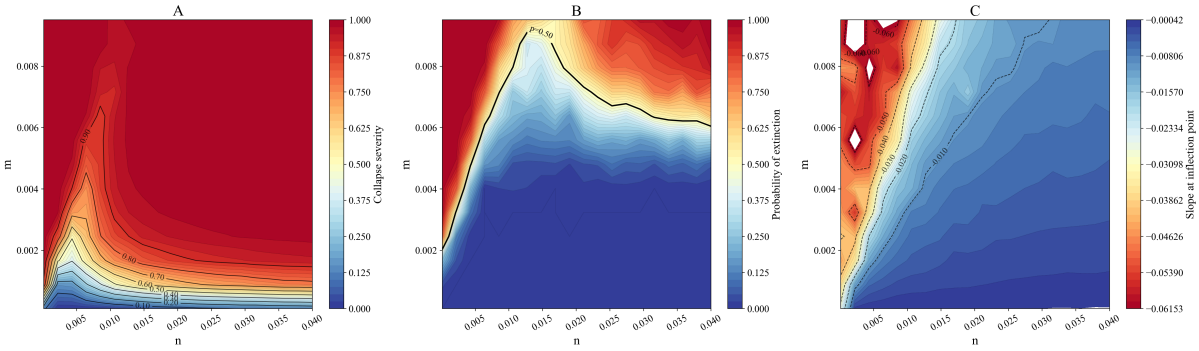

Figure 2: Regime maps in the (n, m) plane, marginalised over the remaining sampled parameters. Panel A shows mean collapse severity; panel B shows extinction probability with the empirical transition boundary at $p = 0.50$; panel C shows the mean slope at the inflection point.

n and m respectively, confirming that stress accumulation modulates collapse outcomes only weakly within the explored domain and does not alter the geometry of the transition identified in the primary regime maps.

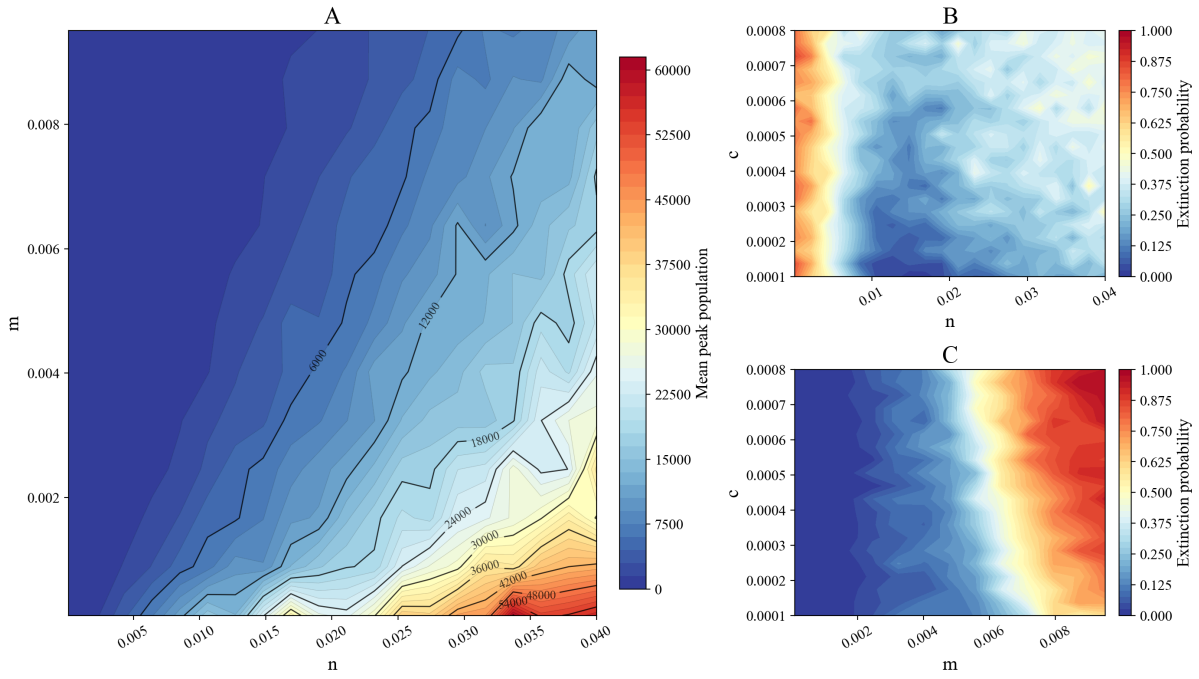

Figure 3: Mean peak population in the (n, m) plane (panel A) and extinction probability in the (n, c) and (m, c) planes (panels B and C), marginalised over the remaining sampled parameters.

4.4. Collapse timing and representative trajectories

The trajectory panels and the $\bar{t}_{\text{peak}}$ heatmap of Figure 4 make explicit the qualitative diversity of dynamic profiles across the parameter space. At $n = 0.001$ and $m = 0.004$, the mean peak time is $\bar{t}_{\text{peak}} = 0$: the population declines immediately from the initial condition, with stochastic realisations converging rapidly toward extinction and no discernible growth phase. At $n = 0.006$, the population grows to a moderate peak at $\bar{t}_{\text{peak}} = 869$, then enters a prolonged and heterogeneous decline in which realisations diverge substantially, reflecting an unstable demographic equilibrium between baseline fertility and stress-mediated reproductive suppression. At $n = 0.015$, a large transient overshoot reaches peaks

of the order of 10^4 individuals before a rapid and convergent collapse at $\bar{t}_{\text{peak}} = 702$, with markedly reduced dispersion among realisations compared to the intermediate regime.

Panel D confirms that these three profiles correspond to structured regions of the parameter space. In the high-m, low-n portion peaks are reached within approximately 350 time steps, indicating rapid collapse with no sustained growth. In the central region peak times range between 500 and 1000 steps, corresponding to the intermediate equilibrium regime. In the low-m, high-n corner $\bar{t}_{\text{peak}}$ exceeds 1500 and in many configurations surpasses the simulation horizon, confirming that the apparent absence of collapse in that region is a consequence of the finite temporal window rather than genuine population stability.

The three dynamic profiles identified in Figure 4 correspond directly to the three regions of the regime map in Figure 2. The direct-collapse regime maps onto the high-severity, high-extinction zone in which the slope at the inflection point is most negative. The intermediate equilibrium maps onto the gradual-decline region in which collapse severity is substantial but extinction within T remains unlikely. The overshoot-collapse maps onto the zone of rapid and abrupt decline identified by the slope indicator in panel C of Figure 2, where large transient peaks are followed by convergent extinction. The coherence between the temporal profiles and the synthetic regime indicators supports the interpretation that the three zones represent genuine and qualitatively distinct dynamic regimes rather than a continuous gradient of outcomes.

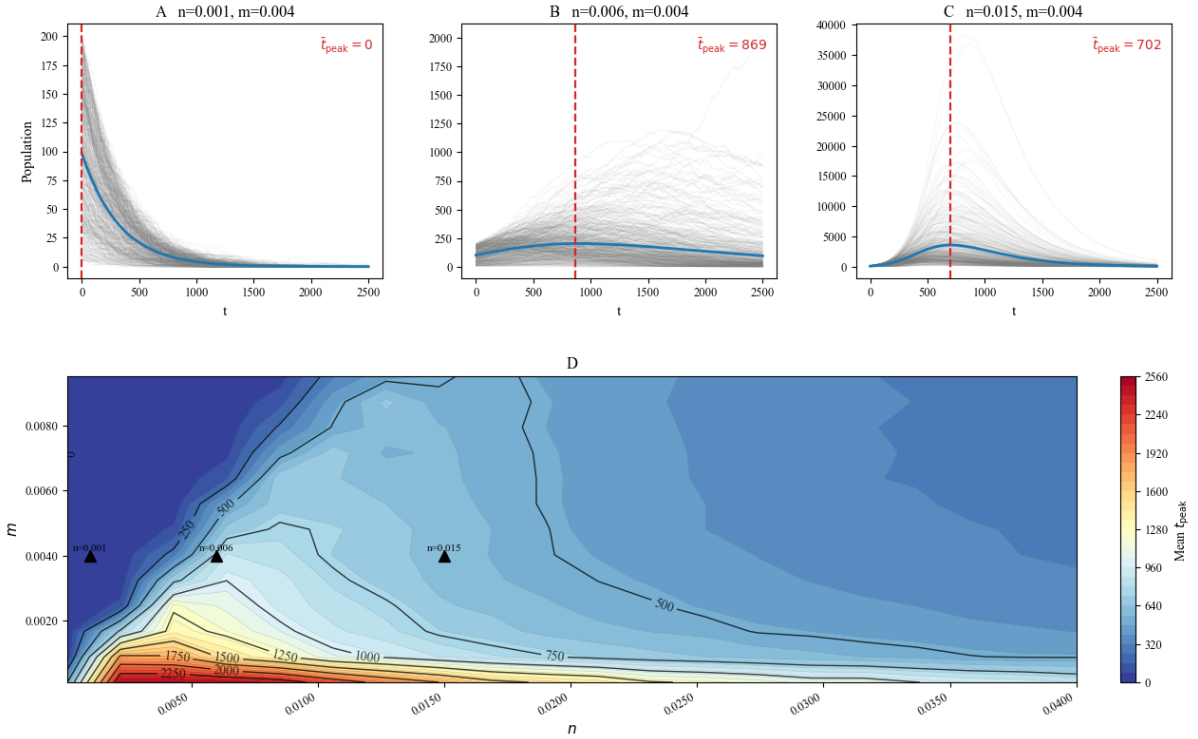

Figure 4: Population trajectories across stochastic realisations for three representative values of baseline fertility at fixed mortality $m = 0.004$ (panels A, B, C), and mean peak time $\bar{t}_{\text{peak}}$ in the (n, m) plane with the three configurations marked (panel D).

5. Discussion and Conclusions

The results support the interpretation of the behavioral sink as a structured collapse mechanism whose geometry can be characterised empirically across the parameter space. Within the explored domain, collapse outcomes are not distributed randomly but organised around a well-defined transition region,

indicating that the emergence of collapse is governed by identifiable demographic conditions rather than by stochastic accident.

The dominant role of mortality m and baseline fertility n in shaping the geometry of this region reflects the centrality of the balance between demographic expansion and stress-constrained reproduction. The effect of n is not direct but amplified by the internal feedback of the model: higher baseline fertility generates larger populations, which in turn produce higher local crowding, accelerate stress accumulation, and ultimately suppress the very fertility that drove initial growth. This nonlinear self-amplifying structure explains why n appears as a strong predictor even though its direct demographic effect is straightforward. At the same time, the remaining parameters — stress accumulation c, fertility suppression k, total space R, number of nodes z, and stress decay d — are not irrelevant in an absolute sense. Their marginal importance within the explored domain reflects the fact that, when m and n vary simultaneously across a wide range, the global geometry of the transition is primarily shaped by these two quantities. The precise position and local curvature of the critical boundary, however, depend on the full parameter configuration, and any species-specific application of the model would require calibrating all parameters rather than only the dominant ones.

The three qualitative regimes identified across the parameter space — direct collapse, stable equilibrium, and overshoot collapse — show that the same causal mechanism produces profoundly different demographic histories depending on the location in the (n, m) plane. In the direct-collapse regime, mortality is so high relative to baseline fertility that the population declines immediately from the initial condition with no discernible growth phase. In the stable equilibrium regime, the population sustains itself over a prolonged period before entering a slow and heterogeneous decline, with high variability among stochastic realisations reflecting the proximity to a demographic balance point. In the overshoot-collapse regime, high baseline fertility allows a large transient peak to develop before stress accumulation becomes sufficient to suppress reproduction below the replacement threshold, after which collapse is rapid and convergent across realisations. These three profiles are not arbitrary outcomes of a stochastic model but correspond to structured and geometrically coherent regions of the parameter space, as confirmed by the coherence between the regime maps and the trajectory analysis.

The model identifies the general demographic conditions under which each regime emerges, but it is designed as a minimal representation of the mechanism rather than as a predictive tool for specific biological systems. Predicting the behaviour of a particular species would require calibrating the internal dynamics of the model — stress accumulation rate, fertility suppression strength, spatial structure — against empirical measurements for that species. This calibration is non-trivial in part because of the discrepancy in timescale and magnitude between the natalità parameters of the model and the reproductive rates of real animal populations, which would require a rescaling of the parameter space before any direct comparison could be attempted.

Two limitations of the present analysis should be acknowledged explicitly. First, the simulation horizon of $T = 2500$ time steps constrains what can be concluded about long-term outcomes. Parameters with slow-acting effects, in particular the stress decay rate d, may become relevant over timescales that exceed the simulated horizon, and the extinction probabilities reported here should be interpreted as lower bounds conditioned on T rather than as definitive assessments of long-term persistence. Second, the empirical transition boundary at $p = 0.50$ identified in the (n, m) plane does not constitute a formal demonstration of bistability or hysteresis in the dynamical-systems sense; it is an operational characterisation of where persistence becomes less likely than extinction within the explored parameter space and the simulated horizon.

This paper provides the first systematic characterisation of the geometry of the critical boundary between survival and collapse regimes in a stochastic agent-based model of the behavioral sink. The three qualitative regimes identified — direct collapse, stable equilibrium, and overshoot collapse — offer a basis for classifying the type of demographic trajectory expected as a function of baseline fertility and mortality, and for anticipating whether a population subject to overcrowding-induced stress is likely to decline gradually, maintain a prolonged equilibrium, or undergo a rapid large-amplitude collapse. The minimal causal structure of the model makes it potentially transferable to other systems in which spatial compression, persistent stress accumulation, and reproductive suppression interact over time,

provided that appropriate parameter rescaling is conducted. Future work should extend the analysis to longer simulation horizons to assess the role of slow-acting parameters, calibrate the model against empirical demographic data for documented animal species while accounting for the discrepancy in reproductive timescales, and incorporate more explicit representations of internal stress dynamics to enable species-specific predictions.

Acknowledgments

The authors thank Andro for the companionship during the writing of this paper and for providing an endless supply of liberty-tea.

Declaration on Generative AI

During the preparation of this work, the author(s) used Claude Sonnet 4.6 (Anthropic) in order to: language editing and LaTeX assistance. After using this tool, the author(s) reviewed and edited the content as needed and take full responsibility for the publication's content.

References

[1] S. Roman, Collapse, in: Dictionary of Ecological Economics, Edward Elgar Publishing, 2023, pp. 72–73.

[2] S. Roman, F. Bertolotti, Global history, the emergence of chaos and inducing sustainability in networks of socio-ecological systems, Plos one 18 (2023) e0293391.

[3] J. B. Calhoun, A behavioral sink, Roots of behavior (1962) 295–315.

[4] J. B. Calhoun, Death squared: the explosive growth and demise of a mouse population, Proceedings of the Royal Society of Medicine 66 (1973) 80–88. URL: https://doi.org/10.1177/00359157730661P202. doi:10.1177/00359157730661P202.

[5] P. D. Edwards, C. Frenette-Ling, R. Palme, R. Boonstra, A mechanism for population self-regulation: Social density suppresses gnrh expression and reduces reproductivity in voles, Journal of Animal Ecology 90 (2021) 784–795.

[6] J. M. V. Respicio, K. C. Dela Cruz, A. C. Hughes, K. C. Tanalgo, The behavioural costs of over-crowding for gregarious cave-dwelling bats, Journal of Animal Ecology 93 (2024) 619–631.

[7] N. M. Haddad, L. A. Brudvig, J. Clobert, K. F. Davies, A. Gonzalez, R. D. Holt, T. E. Lovejoy, J. O. Sexton, M. P. Austin, C. D. Collins, W. M. Cook, E. I. Damschen, R. M. Ewers, B. L. Foster, C. N. Jenkins, A. J. King, W. F. Laurance, D. J. Levey, C. R. Margules, B. A. Melbourne, A. O. Nicholls, J. L. Orrock, D.-X. Song, J. R. Townshend, Habitat fragmentation and its lasting impact on earth's ecosystems, Science Advances 1 (2015) e1500052. URL: https://doi.org/10.1126/sciadv.1500052. doi:10.1126/sciadv.1500052.

[8] C. Fletcher, W. J. Ripple, T. Newsome, P. Barnard, K. Beamer, A. Behl, J. Bowen, M. Cooney, E. Crist, C. Field, et al., Earth at risk: An urgent call to end the age of destruction and forge a just and sustainable future, PNAS nexus 3 (2024) pgae106.

[9] S. Creel, B. Dantzer, W. Goymann, D. R. Rubenstein, The ecology of stress: effects of the social environment, Functional ecology 27 (2013) 66–80.

[10] R.-P. Juster, B. S. McEwen, S. J. Lupien, Allostatic load biomarkers of chronic stress and impact on health and cognition, Neuroscience & Biobehavioral Reviews 35 (2010) 2–16.

[11] B. S. McEwen, H. Akil, Revisiting the stress concept: implications for affective disorders, Journal of Neuroscience 40 (2020) 12–21.

[12] D. Stokols, On the distinction between density and crowding: some implications for future research., Psychological review 79 (1972) 275.

[13] E. T. Hall, E. T. Hall, The hidden dimension, volume 609, Anchor, 1966.

[14] F. Carucci, F. Bertolotti, An agent-based and equation-based meta-model of behavioral sink: the case of universe 25, 2026. Under review at *PNAS*.
[15] V. Grimm, E. Revilla, U. Berger, F. Jeltsch, W. M. Mooij, S. F. Railsback, H.-H. Thulke, J. Weiner, T. Wiegand, D. L. DeAngelis, Pattern-oriented modeling of agent-based complex systems: lessons from ecology, science 310 (2005) 987–991.
[16] M. Edali, G. Yücel, Exploring the behavior space of agent-based simulation models using random forest metamodels and sequential sampling, Simulation Modelling Practice and Theory 92 (2019) 62–81.
[17] S. Gualdi, M. Tarzia, F. Zamponi, J.-P. Bouchaud, Tipping points in macroeconomic agent-based models, Journal of Economic Dynamics and Control 50 (2015) 29–61.
[18] R. Boonstra, Population regulation and limitation—insights from lemming cycles: past, present and future, Proceedings B 291 (2024) 20240660.
[19] P. G. Judge, F. B. M. de Waal, Rhesus monkey behaviour under diverse population densities: coping with long-term crowding, Animal Behaviour 54 (1997) 643–662. URL: https://doi.org/10.1006/anbe.1997.0469. doi:10.1006/anbe.1997.0469.
[20] A. M. Dettmer, M. A. Novak, J. S. Meyer, S. J. Suomi, Population density-dependent hair cortisol concentrations in rhesus monkeys (macaca mulatta), Psychoneuroendocrinology 42 (2014) 59–67. URL: https://doi.org/10.1016/j.psyneuen.2014.01.002. doi:10.1016/j.psyneuen.2014.01.002.
[21] S. Huang, G. Li, Y. Pan, M. Song, J. Zhao, X. Wan, C. J. Krebs, Z. Wang, W. Han, Z. Zhang, Density-induced social stress alters oxytocin and vasopressin activities in the brain of a small rodent species, Integrative zoology 16 (2021) 149–159.
[22] R. I. M. Dunbar, S. Shultz, The infertility trap: The fertility costs of group-living in mammalian social evolution, Frontiers in Ecology and Evolution 9 (2021) 634664. doi:10.3389/fevo.2021.634664.
[23] D. Stokols, A social-psychological model of human crowding phenomena, Journal of the American Institute of Planners 38 (1972) 72–83.
[24] C. B. Stroud, 16 the stress sensitization model, The Oxford handbook of stress and mental health (2019) 349.
[25] F. A. Champagne, M. J. Meaney, Stress during gestation alters postpartum maternal care and the development of the offspring in a rodent model, Biological Psychiatry 59 (2006) 1227–1235.
[26] E. H. Van Nes, B. M. Arani, A. Staal, B. van der Bolt, B. M. Flores, S. Bathiany, M. Scheffer, What do you mean,'tipping point'?, Trends in ecology & evolution 31 (2016) 902–904.
[27] S. M. Munson, S. C. Reed, J. Peñuelas, N. G. McDowell, O. E. Sala, Ecosystem thresholds, tipping points, and critical transitions, New Phytologist 218 (2018) 1315–1317.
[28] V. Dakos, C. A. Boulton, J. E. Buxton, J. F. Abrams, B. Arellano-Nava, D. I. Armstrong McKay, S. Bathiany, L. Blaschke, N. Boers, D. Dylewsky, et al., Tipping point detection and early warnings in climate, ecological, and human systems, Earth System Dynamics 15 (2024) 1117–1135.
[29] S. Roman, S. Bullock, M. Brede, Coupled societies are more robust against collapse: A hypothetical look at easter island, Ecological Economics 132 (2017) 264–278.
[30] A. Hastings, S. Petrovskii, V. Lucarini, A. Morozov, Tipping points in complex ecological systems, arXiv preprint arXiv:2602.20702 (2026).